

# Absolute Rb one-color two-photon ionization cross-section measurement near a quantum interference

T. Takekoshi, G. M. Brooke, B. M. Patterson, and R. J. Knize

*Laser and Optics Research Center, Department of Physics, U.S. Air Force Academy, Colorado 80840, USA*

(Received 4 February 2004; published 20 May 2004)

We observe destructive interference in the ground-state Rb two-photon ionization cross section when the single photon energy is tuned between the  $5S \rightarrow 5P$  and  $5S \rightarrow 6P$  transition energies. The minimum cross section is  $5.9(1.5) \times 10^{-52} \text{ cm}^4 \text{ s}$  and it occurs at a wavelength of 441.0(3) nm (*in vacuo*). Relative measurements of these cross sections are made at various wavelengths by counting ions produced when magneto-optically trapped Rb atoms are exposed to light from a tunable pulsed laser. This relative curve is calibrated to an absolute cross-section measurement at 532 nm using the trap loss method. A simple calculation agrees reasonably with our results.

DOI: 10.1103/PhysRevA.69.053411

PACS number(s): 32.80.Rm, 32.80.Fb, 32.80.Pj

Destructive interference effects in multiphoton ionization were first observed by Morellec and co-workers [1]. Their two-photon experiment had a dense Cs beam source and required laser intensities on the order of  $10^{10} \text{ W/cm}^2$  in order to make atomic ionization (unsaturated) dominate over molecular ionization (partially saturated). Measuring alkali photoionization cross sections using an atomic vapor cell [2] or an atomic beam [1,3] is complicated by geometrical factors and large contributions from alkali dimers. In a thermal beam, the number of  $\text{Rb}^+$  or  $\text{Cs}^+$  ions created by a two-photon ionization of dimers can be 10–100 times larger than from ionization of atoms [3–5]. Using cold, trapped atoms provides a small static sample and allows accurate absolute ionization cross-section measurements to be made using the trap loss method [6]. Because dimers are not trapped, the atom/dimer ratio is high and no extraordinary measures (superheaters, dissociation lasers, etc.) need to be taken to attenuate the dimer contribution. We present here one-color two-photon (linearly polarized) ionization cross sections measured by irradiating magneto-optically trapped  $^{87}\text{Rb}$  atoms with tunable pulsed radiation from an optical parametric oscillator (OPO).

At laser intensities low enough that perturbation theory is valid, the rate  $R_{EJm(l)s,i}$  for an alkali atom in an initial internal bound state  $|i\rangle$  to make a transition to a final free-electron state  $|EJm(l)s\rangle$  in the presence of an electromagnetic mode with angular frequency  $\omega$  and polarization  $\hat{\epsilon}$  can be written as [7–9]

$$R_{EJm(l)s,i} = 8\pi^3 \hbar (\alpha F \omega)^2 \left| \sum_n \frac{\langle EJm(l)s | \hat{\epsilon} \cdot \mathbf{r} | n \rangle \langle n | \hat{\epsilon} \cdot \mathbf{r} | i \rangle}{\omega_{ni} - \omega - i\Gamma_n/2} \right|^2. \quad (1)$$

The sum is over all atomic states  $|n\rangle$ , where  $\hbar\omega_{ni}$  is the energy difference between the intermediate and initial states, and  $\Gamma_n$  is the intermediate-state radiative lifetime.  $E$  is the photoelectron kinetic energy,  $J$  and  $m$  are the total angular momentum quantum numbers,  $l$  is the orbital angular momentum quantum number,  $s$  is the spin quantum number,  $\mathbf{r}$  is the electron position operator, and  $F$  is the photon flux in

$\text{cm}^{-2} \text{ s}^{-1}$ . We have used the normalization convention  $\langle E'J'm'(l's') | EJm(l)s \rangle = \delta_{J'J} \delta_{m'm} \delta_{l'l} \delta_{s's} \delta(E'-E)$ , which makes the density of states  $\rho(E)=1$ . Because of interference between the transition amplitudes for different  $|n\rangle$ , the cross sections  $\sigma_{EJm(l)s,i} = R_{EJm(l)s,i} / F^2$  feature deep minima whose positions are very sensitive to the atomic matrix elements used in Eq. (1).

In the present work, the ion production rates are much smaller than in previous cold atom experiments which use trap loss to measure one-photon ionization rates [6,10–14]. Over almost all of the wavelength range investigated, the ionization induced by the OPO pulses (a few mJ) is too small to have any observable effect on the trap fluorescence. We therefore directly count the ions in order to measure the relative cross sections over the range 423–600 nm. (All wavelengths in this paper are *in vacuo* values.) Ideally, these relative measurements could be made absolute by making an absolute cross-section measurement near the  $5S \rightarrow 6P$  single photon transitions (420.1 and 421.4 nm) where the photoionization rate is large enough to cause trap loss. However, the beating between the longitudinal modes in the OPO pulses is too fast to capture accurately on a detector, which results in absolute multiphoton cross-section measurements that are too high [15]. In addition, drifts in the longitudinal mode structure cause a large scatter in the results [16], which makes multimode radiation undesirable for absolute measurements. We therefore use a high-power, single frequency, pulsed laser at 532 nm to induce magneto-optical trap (MOT) loss. This gives an accurate absolute cross section that fixes the overall scale of our relative measurements. Using a single mode OPO [17] would reduce the scatter in the data and allow the calibration to be done near resonance where high power is not required.

Our tunable radiation source is a 2-ns-pulsed OPO pumped by 355 nm Nd:YAG third harmonic light. The multimode linewidth varies from 11 to 30  $\text{cm}^{-1}$  over the range of wavelengths used. The maximum pulse energy used is 6 mJ. The beam is focused a few cm in front of the MOT. This gives  $1/e^2$  intensity diameters which vary from 1.1 to 2.5 mm depending on the pump power and OPO output wavelength. Since the MOT is about 150  $\mu\text{m}$  in diameter,

corrections for its finite dimensions are negligible ( $\sim 0.2\%$ ). For very small cross sections ( $< 2 \times 10^{-50} \text{ cm}^4 \text{ s}$ ) higher intensities are required and a lens spacer is inserted, moving the focal point closer to the MOT. The ion number is measured with and without the spacer at 437.5 nm (the beginning of this range) to calibrate the geometrical beam changes. (The spacer increases the ion yield up to a factor of 3.) Peak pulse intensities of about  $3 \times 10^8 \text{ W/cm}^2$  are used at the cross-section minimum. The peak intensities used for the 532 nm single frequency absolute cross-section measurement are about  $10^9 \text{ W/cm}^2$ .

Because the ionization rate for excited  $5P$  atoms is usually much higher than that for ground state  $5S$  atoms, the  $5P$  population must be suppressed by switching off the 780 nm MOT lasers during the ionizing pulse [14]. (The  $5P$  atoms undergo one-photon ionization with a cross section on the order of  $10^{-17} \text{ cm}^2$  [6].) The 780 nm lasers are switched off for 150  $\mu\text{s}$  using acousto-optic modulators (AOMs). The OPO pulse occurs 5  $\mu\text{s}$  before the 780 nm lasers are switched back on. We get large extinction ratios by using rf switches to interrupt power to the AOMs (total rf attenuation of 100 dB on each AOM power source). Using AOMs alone, the measured on/off optical power ratio on the far end of a fiber which transports the trapping laser light to the MOT chamber is  $9 \times 10^5$ . The residual light is scattered light from the optical surfaces in the beamline, which enters the fiber. We attenuate it further by a factor of 10–20 by inserting Pockels cells. The optical pumping to  $5P$  resulting from the remaining light is very weak, because the nearest transition is 90 MHz away. (Its frequency is unshifted by the AOM.)

The relative two-photon ionization cross section is measured by collecting ions using a Channeltron electron multiplier biased at  $-4500 \text{ V}$  inside the vacuum chamber. The OPO repetition rate is 30 Hz and ions from 15 000 light pulses are collected for each data point. Time-of-flight discrimination with a multichannel scaler allows us to avoid counting the ions produced from atoms on the chamber windows and interior surfaces. The small background signal due to hot Rb ions is subtracted off. To remove large afterpulsing and gain saturation effects, the ion production rate is set low, and a pulse generator is inserted between the Channeltron and the scaler so that a maximum of one ion per laser pulse can be detected. (The pulse generator's output pulse is wider than the time-of-flight signal range.) By changing the OPO pulse energy as its wavelength is changed, the average number of ions per laser pulse is kept between 0.1 and 0.5 so that Poisson statistics can be applied to accurately add back the correct number of uncounted ions due to double, triple, etc., ion events. Simultaneous measurement of the OPO pulse energy, average laser pulse time profile, and the spatial beam profile allows the relative cross section to be calculated at each wavelength.

Systematic effects such as drifts in the OPO power, fluctuations of the OPO intensity profile at the MOT, and drifts in the trap population are compensated for, by monitoring these parameters while the ions are collected. We sample the ionizing pulse energy during the experiment using a pyroelectric Joulemeter on the beam as it exits the chamber, and calculate the rms value. The beam profile is simultaneously monitored with a calibrated charge-coupled device camera

by sampling the main beam with a beamsplitter upstream from the MOT. An identical path length and focusing lens allow us to monitor the beam diameters at the trap. We use a photodiode to measure and average the trap fluorescence, which is assumed to be proportional to trap population. Average OPO pulse time profiles are taken at several wavelengths using a photodetector and numerically integrated to give the proper two-photon cross sections. Neutral density filters were used to make large changes in OPO intensity, but fine adjustment was done using a thin half-wave retarder and a polarizer to minimize beamsteering effects.

To determine the overall scale of the relative measurements, an absolute measurement is performed at 532 nm. Because the cross section is small here, up to 25 mJ of single frequency pulsed (2 ns) light at 60 Hz is used. This is enough power to have a large effect on the trap population (monitored by measuring the trap fluorescence), which is necessary for the trap loss method [6]. The difference between the trap's unloading and loading rates gives the ionization rate per atom. Five loading/unloading cycles are averaged. The measurement is repeated at six different pulse energies [Fig. 1(c)]. The cross section calculated using these rates, the laser beam spatial profile, the laser pulse time profile, and the rms pulse energy, is divided by the value (at 532 nm) of a curve fit to the relative data taken over the range 460–575 nm. This gives a calibration factor that makes all of the relative data absolute. The fit through the relative data is based on our absolute cross-section calculation presented later in this paper, using a multiplicative factor as a fitting parameter. The fit is limited to this range of data for two reasons: For these wavelengths, the calculated value depends weakly on high-lying intermediate states not included in the calculation. Also, effects due to nonzero laser linewidth are not included in the calculation, and could be important where the curve is steeper. The measured absolute cross section at 532 nm was  $2.29(14) \times 10^{-49} \text{ cm}^4 \text{ s}$ .

In order to verify that one-photon ionization of the residual  $5P$  population is negligible, we measured the ion production rate as a function of OPO pulse energy at the cross-section minimum (441 nm). The fit to the log-log plot shown in Fig. 1(b) has a slope of 1.92(3), which indicates that we are measuring a predominantly two-photon process. (Other runs gave slopes of 1.92 and 2.11, the variation being most likely due to a drift in the laser pulse mode structure.) Using the measured two-photon cross section here, the photon flux, and the one-photon cross section of the excited MOT state [10], we estimate an upper limit on the excited state population of  $10^{-9}$ . (We assume that the number of ions from excited-state ionization is a factor of 10 smaller than the number from two-photon ionization.) Since the wavelength dependence of the one-photon  $5P$  cross section is very weak, and the total trap ion production rate versus wavelength is kept roughly constant by varying the OPO intensity, all other data points are expected to have a negligible one-photon contribution. This is because they use lower photon fluxes than at 441 nm, and will therefore have a lower one-photon rate than at 441 nm. Ion counts taken at 423.6, 425.6, and 440.5 nm also depend quadratically on pulse energy.

For high intensities or for frequencies near resonance, the two-photon atomic absorption can become partially satu-

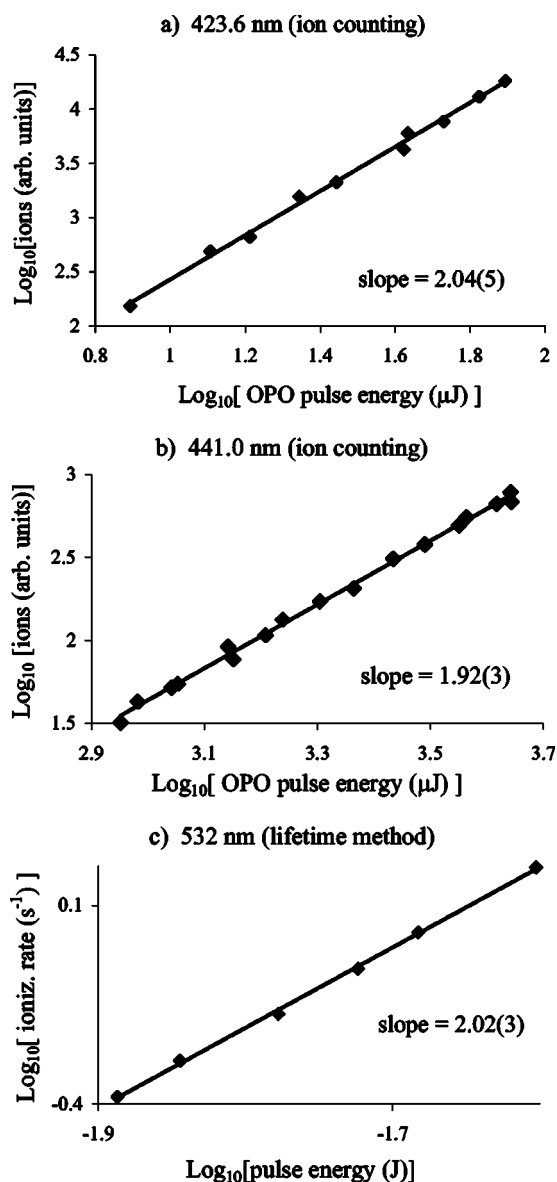


FIG. 1. Collected ions vs pulse energy (log-log) (a) near resonance (relative), (b) at the cross-section minimum (relative), (c) at 532 nm (absolute). The linear fits assume equally weighted points.

rated. (The  $5S \rightarrow 6P$  on-resonance regime has been investigated by Anderlini *et al.* [18].) In order to verify that this did not occur, we measured the dependence of the ionization rate at 423.6 nm near the  $5S \rightarrow 6P$  transition. The fit to the log-log plot of this data shown in Fig. 1(a) has a slope of 2.04(5), which indicates that we are observing an unsaturated two-photon process. High intensity (a few mJ), trap loss measurements were taken at this same wavelength, and were also unsaturated. Quadratic behavior at all wavelengths can be predicted from Fig. 1(b). Saturation requires optical pumping to  $6P$  by the OPO pulse. As the OPO frequency  $\omega$  is tuned, the pumping rate falls off as  $F/(\omega_{6P,5S} - \omega)^2$ , where  $\omega_{6P,5S}$  is the  $5S \rightarrow 6P$  transition frequency. The two-photon cross section falls off faster than this because of interference between the  $5S \rightarrow 5P \rightarrow \text{continuum}$  and  $5S \rightarrow 6P \rightarrow \text{continuum}$  transition amplitudes in Eq. (1). The photon flux  $F$  decreases faster

than  $(\omega_{6P,5S} - \omega)^2$  as our data approach resonance, because the ionization rate is held roughly constant versus wavelength during ion counting. So, since the ionization rate for the points at the cross-section minimum is not saturated [Fig. 1(b)], all of the other data points must be unsaturated as well. Figure 1(c) is evidence that the absolute cross-section calibration measurement at 532 nm was also unsaturated.

The absolute cross-section data are presented in Fig. 2. There are three data runs separated by a few hours each. The largest sources of statistical measurement error in the ion counting cross sections are from the OPO beam profile measurement (1–5%), pulse energy measurement (<1%), MOT fluorescence measurement (1%), and ion counting statistics (<1%). The total statistical error ranges from 2 to 7%. However, the observed scattering in the data is larger than this. The measurements are clearly dominated by an unexplained source of error. This shows up in the ionization vs pulse energy graphs of Figs. 1(a) and 1(b). Each point in these data is taken in the same manner as the points in Fig. 2 but at varying pulse energies. Since the pulse energy and ion counting statistical errors are small, these data can be used to estimate the unexplained cross-section error empirically. Datasets taken at 423.6 [Fig. 1(a)], 425.6 (not shown), 440.5 (not shown), 441.0 nm (not shown), and 441.0 nm [Fig. 1(b)] give cross-section standard deviations of 10, 6, 12, 19, and 7%, respectively. A comparison of measurements at the same wavelength at different times (different data runs) gives even larger discrepancies. The four largest occur at 440.5 nm (factor of 1.8), 460.1 nm (factor of 1.9), 450.3 nm (factor of 2.3), and 479.7 nm (factor of 1.8). The most likely source of this scattering in the data is drifting longitudinal mode structure in the OPO laser [15,16]. There are 13 wavelengths for which the data overlap. Taking the two-point standard deviation, normalizing to the mean, and averaging over the 13 pairs gives an empirical single point standard error of 25%. This should be used as a relative cross-section error. The error in the cross section due to the calibration at 532 nm is 6%. The error in the *in vacuo* wavelength measurement of each point is  $\pm 0.1$  nm in the 400–500 nm range and  $\pm 0.5$  nm at longer wavelengths. The monochromator was calibrated using seven atomic transitions.

The exact minimum was located by scanning the OPO wavelength fast while observing ion production. It lies at 441.0(3) nm. Using the mean value of the two data runs from Fig. 2 at this wavelength, and assigning a 26% (relative and absolute) error, the cross section here is  $5.9(1.5) \times 10^{-52}$  cm<sup>4</sup> s. The OPO laser linewidth here is approximately 12 cm<sup>-1</sup> (0.23 nm), which is not wide enough to produce the flat region observed at the minimum of the data. We therefore expect the data to agree well with calculations that assume a negligible linewidth.

We took one data point at 600.2(5) nm. This is above the two-photon cutoff at 593.6 nm and is due to a three-photon process. The cross section implied by the number of ions collected was  $7.1(1.8) \times 10^{-75}$  cm<sup>6</sup> s<sup>2</sup>. The linewidth of the laser here is 30 cm<sup>-1</sup>.

Calculations of the absolute photoionization cross section of Cs based on Eq. (1) and summing over all intermediate states [19] agree with the data taken by Morellec near the

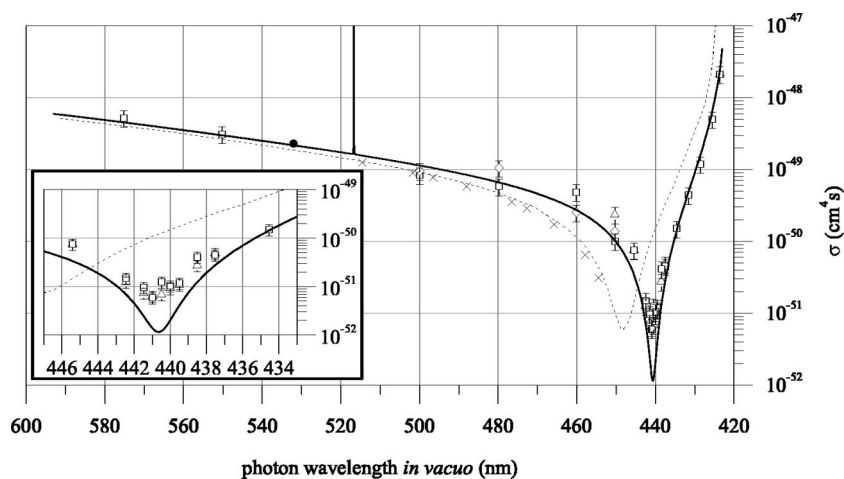


FIG. 2. One-color two-photon ionization cross section of Rb. Open symbols (squares, triangles, and diamonds) are from ion counting measurements (different data runs). The filled circle is the absolute measurement at 532 nm (trap loss method). The dashed curve is the calculation of Bebb reproduced from [8]. The  $\times$  symbols are the calculations of Lambropoulos and Teague [9]. The solid curve is the calculation done in the present work. The disagreement at the minimum is mainly due to the bound-free matrix elements used (extrapolated quantum defect method) and to omission of intermediate states above  $12P$ . The sharp feature at 517 nm is due to the resonant  $5S \rightarrow 4D \rightarrow \text{continuum}$  transition.

minimum at 480 nm [1]. Previous calculations of the absolute cross section of Rb in this wavelength region have been done by Bebb [8] and by Lambropoulos and Teague [9]. They are based on Eq. (1) using a finite number of intermediate states. In both calculations, bound-bound matrix elements are calculated using the quantum defect Coulomb wave-function method of Bates and Damgaard [20], and bound-free matrix elements are calculated using a related method developed by Burgess and Seaton [21]. Our curve in Fig. 2 uses more recent relativistic calculations and experimental results for the bound-bound elements [22–24], but we use the method of Burgess and Seaton to generate the bound-free elements. We sum over the  $5P$  to  $12P$  intermediate states  $|n\rangle$  in Eq. (1). Fine structure is included in the bound states. The effect of spin-orbit coupling on the continuum states is assumed to be negligible, but we use the  $J$  basis here also. Agreement at the calibration point (532 nm) is excellent (within 6%). Near the two-photon threshold (593.6 nm) our curve predicts a cross section of  $\sigma = 6.5 \times 10^{-49} \text{ cm}^4 \text{ s}$ , which agrees with the measurement by Ciampini *et al.* [25] [ $\sigma = 11(6) \times 10^{-49} \text{ cm}^4 \text{ s}$ ]. The only real discrepancy occurs near the cross-section minimum, where the calculation and the data disagree by a factor of 5.

There are several possible reasons for the disagreement at the minimum. Experimentally, there is the possibility that naturally occurring Rb dimers in the (300 K) beam source which feeds the MOT can give a false background signal through the process  $\text{Rb}_2 + \nu \rightarrow \text{Rb}^+ + \text{Rb} + e^-$ . This is the same problem which plagued initial attempts to measure cross sections in Cs near the 480 nm minimum [3]. The 441 nm radiation used near the Rb cross-section minimum lies in the  $D \leftarrow X$  absorption band of  $\text{Rb}_2$  [26,27]. To model the absorption, we assume a three-level system with no ion recombination. From a relative absorption curve [27], and an absolute absorption curve of diffuse bands near 600 nm [28] we estimate the  $\text{Rb}_2$  absorption cross section to be  $2 \times 10^{-17} \text{ cm}^2$  at

440 nm. We assume that the  $D$  state lifetime is 61 ns [4]. We also assume a bound-free cross section similar to that of Rb  $6P$  ( $6 \times 10^{-18} \text{ cm}^2$ ), and a rectangular 2 ns light pulse. Using these parameters, the  $\text{Rb}_2$  two-photon ionization cross section at 441 nm partially saturates and becomes linear with intensity at  $7 \times 10^6 \text{ W/cm}^2$ . At the intensities we used near 441 nm ( $3 \times 10^8 \text{ W/cm}^2$ ), the process is starting to become fully saturated (ionization probability per pulse of about 0.3). Figure 1(b) therefore indicates that there is no significant molecular contribution. Contributions from Cs and  $\text{Cs}_2$  impurities are not detected because they have a different time of flight.

Alternatively, the theory curve at the minimum may not be correct. The calculated minimum in the total cross section shown in Fig. 2 is determined by the sizes and relative displacements (in wavelength) of the minima of the three channels that contribute to the overall rate. The three possible electric dipole-allowed ( $E1-E1$ ) final states are  $|l=0, J=1/2\rangle$ ,  $|l=2, J=3/2\rangle$ , and  $|l=2, J=5/2\rangle$  (Fig. 3). The cross sections for these channels all have minima on the order of  $10^{-64} \text{ cm}^4 \text{ s}$  (Fig. 4). They sum to form a total cross-section curve with a much higher and wider minimum at  $\lambda = 440.6 \text{ nm}$  ( $\sigma = 1.15 \times 10^{-52} \text{ cm}^4 \text{ s}$ ). [The observed minimum occurs at  $\lambda = 441.0(3) \text{ nm}$ ,  $\sigma = 5.9(1.5) \times 10^{-52} \text{ cm}^4 \text{ s}$ ]. Channels with electric quadrupole ( $E2$ ) and magnetic dipole ( $M1$ ) matrix elements, may be significant at the minimum. The most significant are the channels utilizing bound-bound  $E2$  and  $M1$  matrix elements. Channels utilizing bound-free  $E2$  and  $M1$  transitions will have a minimum near 441 nm for the same reason one exists there for the  $E1-E1$  channels.

To calculate the contribution of the  $E2-E1$  channels we use the  $5S-4D$  oscillator strength measurements of Nilsen and Marling [29]. The prediction of Warner [30] that the  $5S-5D$  matrix element is negligible allows us to make the approximation that only the  $4D$  term is significant at 441 nm. We find, however, that the total contribution from these

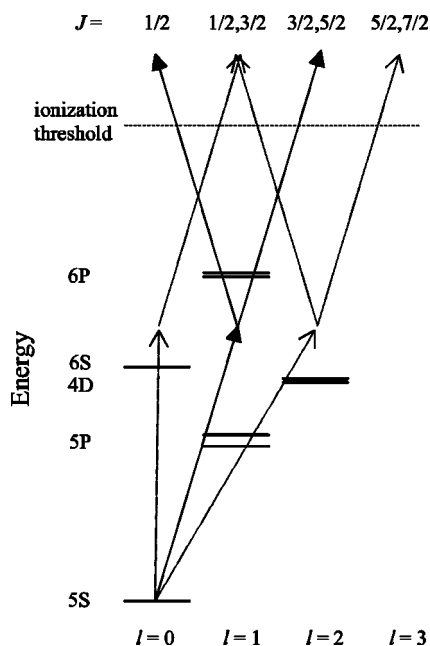


FIG. 3. Electric dipole allowed ( $E1-E1$ , heavy arrows) and partially disallowed ( $E2-E1$  and  $M1-E1$ , light arrows) two-photon ionization transitions in Rb.

channels at 441 nm is only  $1.7 \times 10^{-56} \text{ cm}^4 \text{ s}$ , but dominates in a very narrow range near the  $5S-4D$  resonance at 517 nm (The peak is  $2 \times 10^{-40} \text{ cm}^4 \text{ s}$  in the low intensity limit). This has been observed experimentally by Dodhy *et al.* [31].

The contribution of the  $M1-E1$  channels was estimated based on relativistic calculations of the  $M1$   $5S-6S$  matrix element (neglecting the off-diagonal hyperfine contribution) [32]. The contribution at 441 nm is on the order of  $10^{-67} \text{ cm}^4 \text{ s}$ . The contribution on resonance at 497 nm is on the order of  $10^{-56} \text{ cm}^4 \text{ s}$ . The contribution at 441 nm of the larger  $5S-5S$  hyperfine  $M1$  transitions is about  $10^{-65} \text{ cm}^4 \text{ s}$ .

The effects of electrostatic  $S-P$  mixing due to the ion collection field, and the cross section for the simultaneous absorption of two photons (with no intermediate state) were also investigated and found to be negligible.

Another possible explanation for disagreement at the minimum is that the bound-free elements calculated using the Burgess and Seaton method are not good enough to predict the cross section here. (The bound-bound elements are

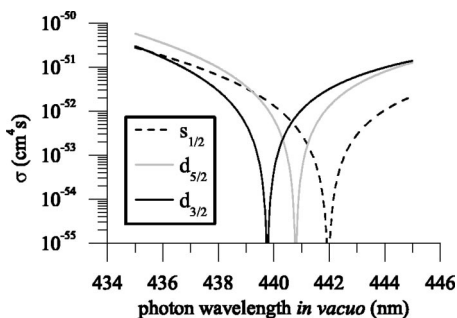


FIG. 4. Calculated photoionization cross sections for the three electric dipole allowed ( $E1-E1$ ) channels near the total cross-section minimum.

known to better than 1%.) Arbitrary 10% adjustments in either the  $5P$  or  $6P$  bound-free elements of a single channel can change the position of its minimum by more than 1 nm, which can have a large effect on the size of the total cross-section minimum (up to a factor of 3), while having a much smaller or even negligible effect away from the total cross-section minimum. Although these elements depend continuously on the photoelectron energy (and thus the radiation wavelength), they can be compared with experimental results at specific energies. The sum of the squares of the elements from each channel is proportional to the total one-photon excited-state ionization cross section.

Dineen *et al.* measured the  $5P_{3/2}$  single-photon ionization cross sections at 413 and 407 nm [6]. We can calculate these cross sections using our  $5P_{3/2} \rightarrow \text{continuum}$  elements. At 413 nm (corresponding to a two-photon wavelength of 540 nm) the measured and calculated one-photon cross sections are  $1.36(12)$  and  $1.12 \times 10^{-17} \text{ cm}^2$ , respectively. At 407 nm (corresponding to a two-photon wavelength of 535 nm) the measured and calculated one-photon cross sections are  $1.25(11)$  and  $1.10 \times 10^{-17} \text{ cm}^2$ , respectively. This is of limited usefulness since we really need to know the accuracy of these elements near the two photon cross-section minimum (441 nm). Also, the magnitude of the total two-photon cross section at the minimum depends strongly on the relative sizes and wavelength splittings between the  $s_{1/2}$ ,  $d_{3/2}$ , and  $d_{5/2}$  cross-section minima, which was not measured.

Gabbanini *et al.* measured the Rb  $5P_{3/2}$  single-photon ionization cross section at 476.5 nm to be  $1.48(22) \times 10^{-17} \text{ cm}^2$  [10]. This corresponds to a two-photon wavelength of 591.6 nm. Using the  $5P_{3/2} \rightarrow \text{continuum}$  Burgess and Seaton elements to calculate this cross section gives  $1.28 \times 10^{-17} \text{ cm}^2$ . By using circularly polarized light, the ratio of the  $s$  and  $d$  one-photon  $5P_{3/2}$  cross sections  $\sigma_s/\sigma_d$  for linearly polarized light at 476.5 was measured by the same group to be 0.176 (uncertainty not published) [33]. The ratio predicted using our Burgess and Seaton elements is 0.122.

Ambartzumian *et al.* measured the Rb  $6P$  single-photon ionization cross sections at 694.3 nm (corresponding to a two-photon wavelength of 523.6 nm) [34]. The measured and calculated  $6P_{1/2}$  cross sections are  $1.7(4)$  and  $1.11 \times 10^{-17} \text{ cm}^2$ , respectively. The measured and calculated  $6P_{3/2}$  cross sections are  $1.5(4)$  and  $1.08 \times 10^{-17} \text{ cm}^2$ , respectively.

The Rb two-photon  $s$  wave to  $d$  wave cross-section ratio has been measured by Wang and Elliott at nine wavelengths from 590 to 532 nm by observing the angular distribution of ejected photoelectrons using elliptically polarized light [35,36]. (Also see note added at the end of Ref. [37].) Their measured  $s$  to  $d$  cross-section ratios for linearly polarized light do not agree well with those predicted by our calculation. Their values are smaller by a factor of 2.3 at 590 nm. The disagreement grows gradually to a factor of 4 at 532 nm. Their ratios are about a factor of 2 smaller than those predicted by Colgan and Pindzola [37] using relativistic perturbation theory with fine structure. Colgan and Pindzola's results for the  $d_{5/2}$  wave to  $d_{3/2}$  wave cross-section ratio are consistent with those expected if fine structure effects are small in the continuum states.

Given these comparisons with experimental data, and the fact that 10% single element bound-free adjustments in a

single channel can have a large effect near 441 nm, the limited accuracy of these elements probably makes a major contribution to the factor of 5 disagreement between theory and experiment at the total cross-section minimum. The omission of the bound states above  $12P$  and of the continuum intermediate states in Eq. (1) is also important, but is not likely to change the calculated cross section at the minimum by more than a factor of 2 [38].

In summary, we have measured the absolute two-photon

ionization cross section of Rb near a quantum interference minimum for the first time. Because we used cold-trapped atoms, the accuracy is higher and the laser intensities required are two orders lower than those used in the analogous Cs experiment [1]. A simple calculation agrees well with our data everywhere except at the minimum.

This work was funded by National Science Foundation Grant No. 9988100 and the Air Force Office of Scientific Research.

- 
- [1] J. Morellec, D. Normand, G. Mainfray, and C. Manus, *Phys. Rev. Lett.* **44**, 1394 (1980).
- [2] J. A. R. Samson, *Adv. At. Mol. Phys.* **2**, 177 (1966).
- [3] E. H. A. Granneman and M. J. V. der Wiel, *J. Phys. B* **8**, 1617 (1975).
- [4] E. H. A. Granneman, M. Klewer, K. J. Nygaard, and M. J. V. der Wiel, *J. Phys. B* **9**, 865 (1976).
- [5] E. H. A. Granneman, M. Klewer, and M. J. V. der Wiel, *IXth International Conference on the Physics of Electronic and Atomic Collisions* (University of Washington Press, Seattle, 1975), Part I, p. 471.
- [6] T. P. Dineen, D. Wallace, and P. L. Gould, *Opt. Lett.* **17**, 1706 (1992).
- [7] H. B. Bebb and A. Gold, *Phys. Rev.* **143**, 1 (1966).
- [8] H. B. Bebb, *Phys. Rev.* **149**, 25 (1966).
- [9] P. Lambropoulos and M. R. Teague, *J. Phys. B* **9**, 587 (1976).
- [10] C. Gabbanini, S. Gozzini, and A. Lucchesini, *Opt. Commun.* **141**, 25 (1997).
- [11] O. Maragò, D. Ciampini, F. Fuso, E. Arimondo, C. Gabbanini, and S. T. Manson, *Phys. Rev. A* **57**, R4110 (1998).
- [12] B. M. Patterson, T. Takekoshi, and R. J. Knize, *Phys. Rev. A* **59**, 2508 (1999).
- [13] B. C. Duncan, V. Sanchez-Villicana, P. L. Gould and H. R. Sadeghpour, *Phys. Rev. A* **63**, 043411 (2001).
- [14] J. R. Lowell, T. Northup, B. M. Patterson, T. Takekoshi, and R. J. Knize, *Phys. Rev. A* **66**, 062704 (2002).
- [15] J. L. DeBethune, *Nuovo Cimento Soc. Ital. Fis., B* **12B**, 101 (1972).
- [16] C. Lecompte, G. Mainfray, C. Manus, and F. Sanchez, *Phys. Rev. Lett.* **32**, 265 (1974).
- [17] J. Mes, M. Leblans, and W. Hogervorst, *Opt. Lett.* **27**, 1442 (2002).
- [18] M. Anderlini, E. Courtade, D. Ciampini, J. H. Müller, O. Morsch, and E. Arimondo, *J. Opt. Soc. Am. B* **21**, 480 (2004).
- [19] G. Laplanche, M. Jaouen, and A. Rachman, *J. Phys. B* **16**, 415 (1983).
- [20] D. R. Bates and A. Damgaard, *Philos. Trans. R. Soc. London, Ser. A* **242**, 101 (1949).
- [21] A. Burgess and J. J. Seaton, *Mon. Not. R. Astron. Soc.* **120**, 121 (1960).
- [22] M. S. Safronova, W. R. Johnson, and A. Derevianko, *Phys. Rev. A* **60**, 4476 (1999).
- [23] U. Volz and H. Schmoranzner, *Phys. Scr., T* **T65**, 48 (1996).
- [24] J. Migdalek and Y. Kim, *J. Phys. B* **31**, 1947 (1998).
- [25] D. Ciampini, M. Anderlini, J. H. Mueller, F. Fuso, O. Morsch, J. W. Thomsen, and E. Arimondo, *Phys. Rev. A* **66**, 043409 (2002).
- [26] N. Gador, B. Zhang, R. Andersson, P. Johansson, and T. Hansson, *Chem. Phys. Lett.* **368**, 202 (2002).
- [27] R. Gupta, W. Happer, J. Wagner, and E. Wennmyr, *J. Chem. Phys.* **68**, 799 (1978).
- [28] G. Pichler, S. Milošević, D. Veža, and R. Beuc, *J. Phys. B* **16**, 4619 (1983).
- [29] J. Nilsen and J. Marling, *J. Quant. Spectrosc. Radiat. Transf.* **20**, 327 (1978).
- [30] B. Warner, *Mon. Not. R. Astron. Soc.* **139**, 115 (1968).
- [31] A. Dodhy, R. N. Compton, and J. A. D. Stockdale, *Phys. Rev. A* **33**, 2167 (1986).
- [32] I. M. Savukov, A. Derevianko, H. G. Berry, and W. R. Johnson, *Phys. Rev. Lett.* **83**, 2914 (1999).
- [33] C. Gabbanini, F. Ceccherini, S. Gozzini, and A. Lucchesini, *J. Phys. B* **31**, 4143 (1998).
- [34] R. V. Ambartzumian, N. P. Furzikov, V. Letokhov, and A. A. Puretsky, *Appl. Phys.* **9**, 335 (1976).
- [35] Z. Wang and D. S. Elliott, *Phys. Rev. A* **62**, 053404 (2000).
- [36] Z. Wang and D. S. Elliott, *Phys. Rev. Lett.* **84**, 3795 (2000).
- [37] J. Colgan and M. S. Pindzola, *Phys. Rev. Lett.* **86**, 1998 (2001).
- [38] M. Aymar and M. Crance, *J. Phys. B* **15**, 719 (1982).